Nuclear Materials and Energy 47 (2026) 102135

Contents lists available at ScienceDirect

Nuclear Materials and Energy

journal homepage: www.elsevier.com/locate/nme

First evidence of helium in the tungsten divertor of the WEST tokamak

M. Diez [a], C. Martin [b], A. Hakola [c], A. Huart [a], Y. Corre [a], J. Gaspar [d], Z. Siketić [e], G. Giacometti [b], T. Neisius [f], M. Cabié [f], Q. Tichit [a], T. Vuoriheimo [c], A. Benmoumen [b], E. Tsitrone [a], I.Bogdanovic Radovic [e,*], the WEST team [1]

[a] CEA, IRFM, F-13108 Saint-Paul-Lez-Durance, France
[b] Aix Marseille Univ, CNRS, PIIM, Marseille, France
[c] VTT Technical Research Centre of Finland Ltd, POBox 1000, FI-02044 VTT, Finland
[d] Aix-Marseille Univ, CNRS, IUSTI, Marseille, France
[e] Ruđer Bošković Institute, Bijenička 54, 10000 Zagreb, Croatia
[f] Aix-Marseille Univ, CNRS, CP2M, Marseille, France

ARTICLE INFO

Keywords:
Helium
Tungsten
WEST tokamak
Nanobubbles
Implantation

ABSTRACT

ITER will operate with plasma-facing materials made of tungsten, a material whose surface morphology changes when exposed to helium plasmas at sufficient high energy, fluence and surface temperature. To predict any potential changes to tungsten in future fusion reactors, a dedicated helium campaign was carried out in WEST in 2019. The plasma scenarios developed during this campaign were aimed in particular at forming tungsten fuzz on the surface of tungsten-coated graphite divertor components. A large-scale post-mortem study reveals for the first time the radial and toroidal distributions of helium content in the components determined post-mortem by ion beam analysis at the divertor scale. The results show that helium is mainly found in tungsten at the strike point areas, with concentrations reaching up to 10 at.% near the surface to an analysed depth of 0.2 μm. This is accompanied by the presence of nanobubbles in the microstructure up to 10 nm below the surface observed by electron microscopy. The same observation was made in bulk tungsten ITER-like PFUs. However, no tungsten fuzz was observed.

Introduction

According to the new ITER baseline plan, helium may be used with hydrogen plasmas during the Start of Research Operation (SRO) phase to demonstrate H-mode operation without activating the in-vessel components and will also be produced during DT operations [1]. Depending on the plasma conditions and the surface temperature, the helium flux interacting with the tungsten (W) plasma-facing components (PFCs), and more particularly on the lower divertor (the most loaded area) could lead to surface modifications. Indeed, interactions between helium plasma and W material could induce changes to the nanostructure of the surface and the near-surface region, such as the formation of dislocation loops, bubbles and holes resulting from bursting bubbles and formation of nanodentrils (also known as 'fuzz') as already demonstrated in linear devices [2–4], in Alcator C-Mod [5] and more recently in ASDEX Upgrade [6]. This could lead to enhanced erosion as well as dust formation and should therefore be avoided in a fusion power plant.

In order to consolidate ITER divertor performance and lifetime predictions regarding He/W interactions, a dedicated helium (He) campaign was carried out during the course of the 2019 (C4) campaign in the WEST tokamak. More specifically, the aim was to achieve the plasma conditions required to form W fuzz in the inertially cooled W-coated graphite divertor tiles.

A previous study [7] reported that the conditions were marginally reached in the outer strike point area of these tiles in WEST but erosion seemed to dominate over fuzz formation based on preliminary observations at the time. Since then, an extensive post-mortem analysis has been carried out on the lower divertor targets and obtained results are presented here.

* Corresponding author.
E-mail address: iva@irb.hr (I.Bogdanovic Radovic).
[1] See http://west.cea.fr/WESTteam

https://doi.org/10.1016/j.nme.2026.102135
Received 13 March 2026; Received in revised form 17 April 2026; Accepted 28 April 2026
Available online 28 April 2026
2352-1791/© 2026 The Authors. Published by Elsevier Ltd. This is an open access article under the CC BY license (http://creativecommons.org/licenses/by/4.0/).

Experimental details

Description of the helium campaign

The 2019 (C4) campaign in WEST was divided into a D_2 and a He campaign. The beginning of the He campaign was devoted to He-D_2 changeover studies while the end of the campaign was dedicated solely to He experiments. During this last phase, up to 174 repetitive pulses (#55813 to #55987) were performed on the lower divertor during a full week of plasma operation, corresponding to about 33 min of He plasma exposure and 4.4 GJ of injected energy. The aim of the second part of the campaign was to reach the conditions necessary for fuzz formation in W which could be summarized as follows: $T_{surf} > 700°C$, He fluence $> 10^{24}$ He/m^2 and incident He energy > 20 eV [8–10].

At the time of the helium campaign, the lower divertor consisted of inertial W-coated graphite tiles (identified as W/graphite PFUs in this paper) and a few actively cooled ITER-like PFUs made of bulk W monoblocks [11]. The experiment specifically targeted 1) W/graphite PFUs for which the surface temperature can more easily reach high temperatures in steady state compared to actively cooled W monoblocks and 2) the outer strike point (OSP) region of W/graphite PFUs located in the maximum ripple position due to highest particle loads.

The surface temperature of the W/graphite PFUs was monitored using integrated thermocouples (TC), fibre Bragg gratings (FBG) and infrared (IR) cameras. During the whole C4 campaign, their temperature remained in the range of 70°C to 830°C in steady state and regularly exceeded 500°C during the helium campaign (see Fig. 4 of [12]). However, fuzz begins to form when the surface temperature reaches 700°C or more, which did not occur significantly during the 174 pulses. Based on the considerations in [7], it generally takes about 20 s for the W/graphite PFUs to reach 700°C at the OSP in steady state (shot #55953). Of the 174 pulses of the He campaign, this represents a cumulated total duration of 100 s. This value was used to calculate the fluence.

As for the ITER-like PFU, it was not equipped with TC or FBG. Its surface temperature could only be derived from IR data and usually did not exceed 300-400°C at the center of the monoblock [13]. Because it is impossible to evaluate the cumulated time during which W reached 700°C or more, and for sake of simplicity, the value of 100 s was also used in the fluence calculation (although it is clearly less than 100 s).

Local plasma conditions were monitored using an array of Langmuir probes (LP) embedded in the divertor at toroidal positions that correspond to the maximum of the ripple effect on the inner and outer sides. The particle fluence was recalculated in this paper using magnetic reconstruction and updated data from the LP. The parallel ionic flux was calculated from the ion saturation current and the angle of the local magnetic field relative to the surface of the probes. Since the main ion is helium, the charge state of the ions must be taken into account and a factor of 1 (for the assumption that only He^+ strike the divertor) or 0.5 (for the assumption that only He^{2+} strike the divertor) was used to convert the ion saturation current to the particle flux (He flux in the order of 1-5x10^{22} m^2/s). I.e., the "He^+ only" fluence is exactly twice the "He^{2+} only" fluence (see Fig. 3 and 6). Assuming the toroidal symmetry of the parallel ionic flux ($\Phi_{//}$), the parallel ionic flux calculated on the maximum particle flux areas is used to calculate the perpendicular ionic flux on the divertor at the desired toroidal position using the angle of the local magnetic field relative to the PFC surface ($\Phi_n = \Phi_{//} \bullet \sin\alpha$), α being comprised between 1.5° and 3.5° [14]. The fluence was calculated by integrating the perpendicular ionic flux (Φ_n) in time above 700°C (i.e., 100 s).

The position of the strike point (SP) was derived from magnetic reconstruction (and is therefore subject to uncertainty of a few mm to cm). There is a 'natural' offset between the position of the SP and the position of the heat and particle flux due to the diffusion of the scrape-off layer in the private region (a few mm at least).

Analysed specimens

Although the experiment was targeting more specifically W/graphite PFUs, both types of divertor targets (W/graphite PFUs and ITER-like PFUs) were characterized during post-mortem analyses in order to obtain comparative information between coated W and bulk W with respect to their interactions with helium.

3 divertor targets were dismounted during the shutdown right after the helium campaign and cut into smaller samples for post-mortem analysis:

- 2 W/graphite PFUs from Q4A sector (representing 30 samples)
- 1 ITER-like PFU from Q3B sector (monoblocks 2, 5,6,7,10,13,15,16,25,26,28 and 32)

For the sake of comparison, these tiles shared the same plasma history, i.e. they were exposed to the C3 + C4 campaigns.

The inner and outer W/graphite PFUs were located in areas of maximum plasma loading in the ripple pattern where maximum heat and particle flux is expected (inner tile on toroidal position #7 corresponding to maximum ISP and outer tile on toroidal position #18 corresponding to maximum OSP; see Fig. 1(b)). They had a toroidal bevel on their surface. They were cut into 17 mm diameter samples (17 samples from the inner PFU, 13 samples from the outer PFU).

On the other hand, the ITER-like PFU used in the present study was located in toroidal position #13, which does not correspond to a maximum loading in the ripple pattern. However, it had a flat top geometry (no toroidal bevel) and was vertically misaligned with respect to its upstream neighbor, thus exposing its leading edge (LE) to intense plasma loading. 12 monoblocks were extracted from the ITER-like PFU to serve as samples for this study. Other analyses were performed on this ITER-like PFU and are reported in [11,15–17].

Each sample is identified either by the monoblock (MB) number or by an 's' coordinate, running from high field side (HFS) to low field side (LFS) (see Fig. 1(b)).

Analysis methods

After dismantling and cutting the divertor targets, Ion Beam Analysis (IBA) technique Time-of-Flight Elastic Recoil Detection Analysis (TOF ERDA) and electron microscopy techniques Scanning Electron Microscopy/Transmission Electron Microscopy (SEM/TEM) were used to characterize the helium inventory and structural changes in W, respectively.

The W/graphite PFU samples and the MB samples were first analysed by TOF ERDA. TOF ERDA is the only IBA technique and in general one of the rare techniques that can provide information on the concentration (in at.%) and depth distribution of He in the first 100–150 nm of the sample, which is more than the expected implantation depth for He (usually 1 to tens of nm depending on the energy of He ions [18]). Some of other techniques that can give information about He trapped in the sample are i) thermal desorption spectroscopy [19,20], which is very often not possible to perform while it requires very high temperatures, ii) glow discharge optical emission spectroscopy [21] that needs to be calibrated against known reference samples and iii) laser induced breakdown spectroscopy that needs for quantification help of some other techniques [22,23]. However, none of these techniques can give at the same time quantitative information about the concentration of He as well as depth distribution in the first 150–200 nm of the sample.

The measurements were carried out at 6 MV Tandem Van de Graaff accelerator located at Ruđer Bošković Institute using 23 MeV $^{127}I^{8+}$ ions with 20° incidence angle toward the sample surface. TOF ERDA spectrometer was positioned at an angle of 37.5° toward the beam direction [24,25]. Beam size spot at the target was about 2×3mm^2. In addition of He, also H, D, B, C, N, O, F, W as well as traces of Cr, Fe and Cu were determined in most of the samples. Analysis of TOF-ERDA spectra was

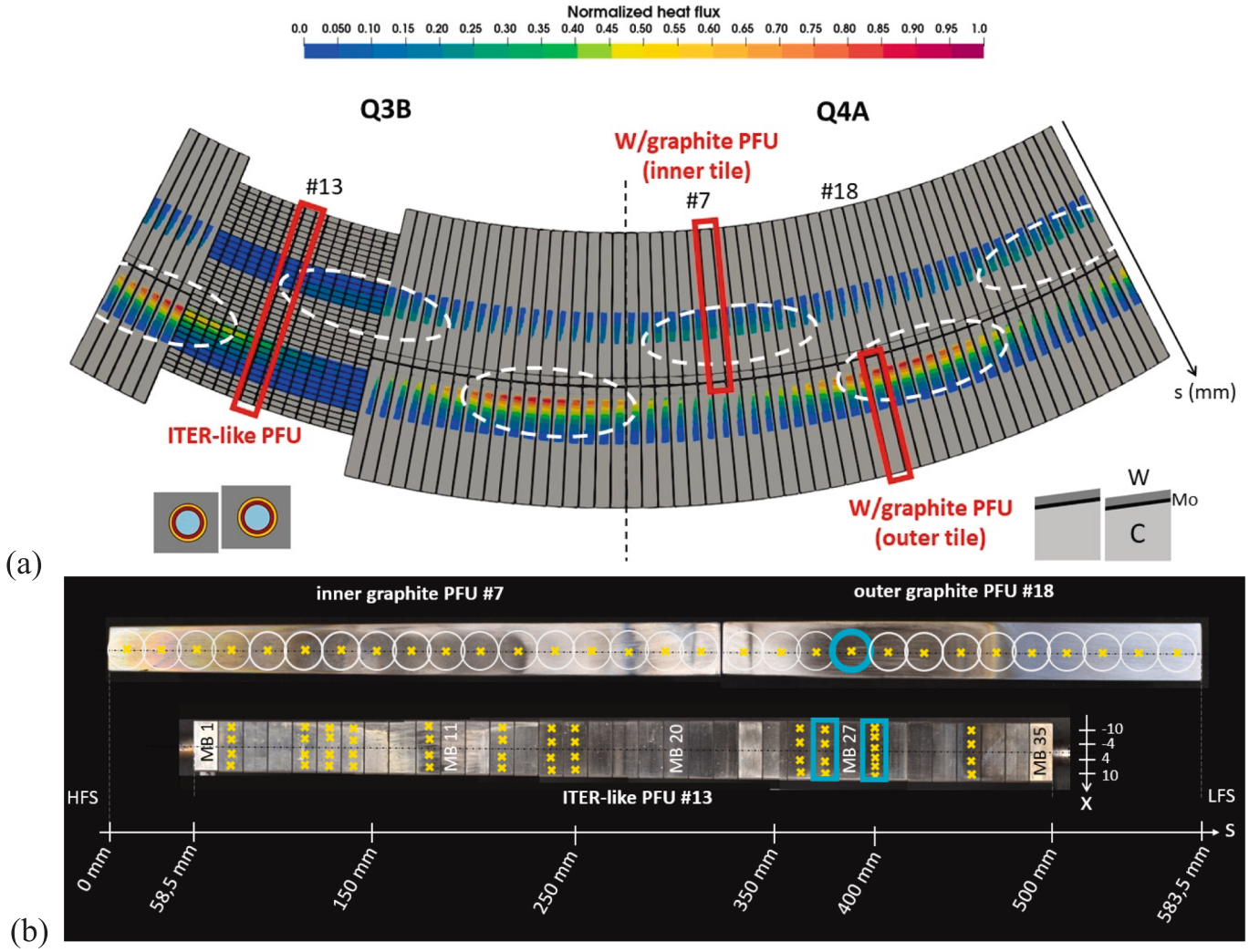

Fig. 1. (a) Location of the three tiles investigated in this study (W-coated graphite PFUs and bulk W ITER-like PFU) with regard to the heat and particle flux modulation on the lower divertor sectors. (b) Cutting scheme and identification of the samples – yellow crosses indicate the location of IBA measurements while blue contours indicate the samples analysed by SEM/TEM to visualize changes in the microstructure. (For interpretation of the references to colour in this figure legend, the reader is referred to the web version of this article.)

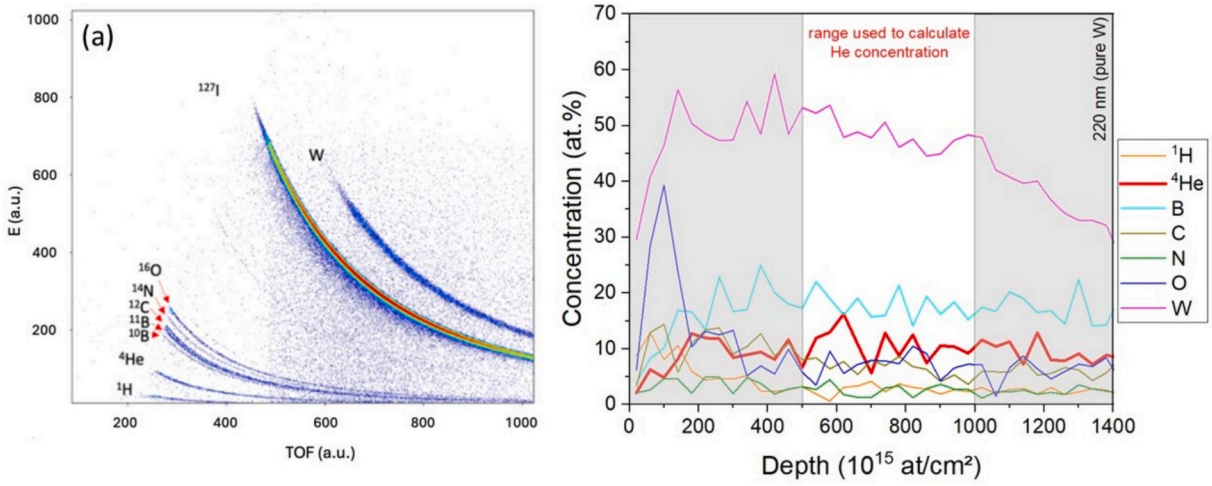

Fig. 2. (a). TOF ERDA spectrum obtained on a W/graphite PFU sample (OSP, s=395 mm) showing the 2D time-of-flight vs. energy spectra. (b) The concentration of all elements present in the sample can be calculated by projecting to TOF axis all elements found in the sample and by normalizing them to 100% in the region between (500–1000)x10^{15} at/cm^2.

done using program Potku [26]. To obtain depth profiles, normalisation to 100% was performed between 500x10^{15}at/cm^2 to 1000x10^{15} at/cm^2 depth, which is shown on Fig. 2.(b) as a white region. It is important to note that TOF ERDA determines depths in at/cm^2, not in nanometres.

For the W/graphite PFUs, measurements were made at the centre of each of the 30 samples, providing a helium content over a radial profile, from HFS to LFS. For the ITER-like PFU, measurements were performed on 12 selected MBs. On each monoblock, four measurements were performed in the toroidal direction (x = -10, −4, 4, 10 mm; x = 0 being the centre of the monoblock), except for MB28 where 9 measurements were performed for other purposes [15].

The samples with the highest helium content were then selected for further investigation using electron microscopy. The surface of the selected samples was first examined using a confocal microscope (SensoFar S Neox, 3D optical profilometer) to analyse the surface topography and identify areas of interest. The surface was then observed by SEM (Zeiss Gemini SEM500) and thin lamellae were extracted using a dual beam focused ion beam (FEI Helios 600 NanoLab) by depositing Pt coating on the surface to prevent damage near the surface. Cross-sectional observations of the lamellae were carried out using TEM (FEI Titan 80–300) at an acceleration voltage of 200 kV to visualize nanostructures below the surface.

Results and discussion

Measurement of helium concentration

Fig. 2 shows results obtained by TOF ERDA in one of the W/graphite PFU sample (OSP, s = 395 mm), providing a better understanding of how the concentration values given in this paper were obtained.

Fig. 2(a) shows the obtained 2D energy versus time-of-flight spectra of the sample while Fig. 2(b) shows the extracted depth profiles. The concentration of all elements present in the sample is calculated by projecting all elements found in the sample onto the TOF axis and normalizing to 100% in the range between (500–1000)x10^{15} at/cm^2 in order to avoid surface effects and decay at higher depth.

As can be seen in Fig. 2(b), the concentration of all elements with depth is homogeneous (N originates from the injection during the current ramp-up), with the exception of O, which shows a strong peak at the surface. Although the concentration of W appears to decrease with depth, this is not the case. This is due to multiple scattering of the recoils traveling from the sample to the detector. The effect is more pronounced for heavier than for lighter recoils, resulting in a higher number of undetected W recoils, especially if they come from greater depths.

Helium content along the W/graphite PFUs and ITER-like PFU

Fig. 3 (a,c) shows distribution of the helium concentration (calculated as described in the previous paragraph) and He content obtained by TOF ERDA along the W/graphite PFUs and the ITER-like PFU. For each sample, the total He content (in 10^{20} at/m^2) was calculated by integrating the number of He atoms from the sample surface to the total measurable depth of about 1400x10^{15} at/cm^2 (corresponding to 220 nm of pure W). However, each sample has different composition and unknown density so conversion from 10^{15} at/cm^2 to nm is not easy.

For the W/graphite PFUs (Fig. 3(a)) it can be seen that significant

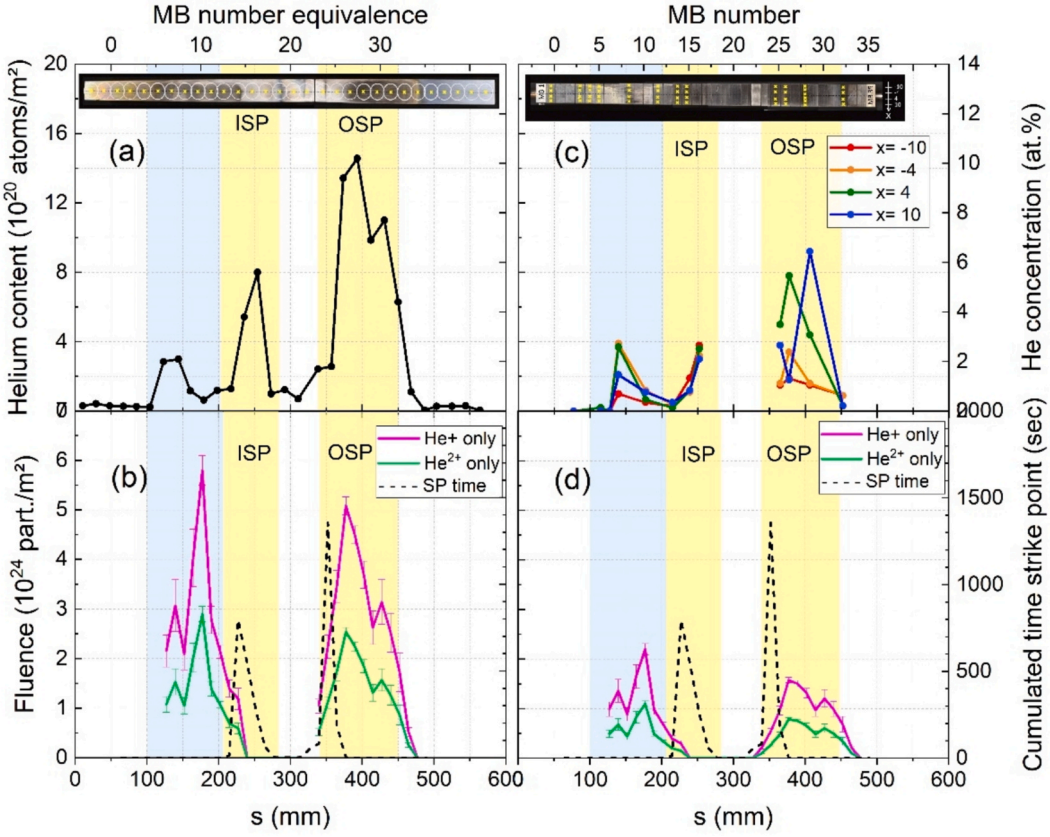

Fig. 3. (a,c) Helium concentration and content measured by TOF ERDA along the W/graphite PFUs and the ITER-like PFU, respectively, after the helium campaign. For the ITER-like PFU, measurements were also performed along the toroidal direction on each monoblock (x = -10,-4,4,10 mm), the x-scale is visible in the inset but also in figure 1b. (b,d) Cumulated He fluence along the W/graphite PFUs and the ITER-like PFU over the 100 s of the helium campaign during which surface temperature was > 700°C. Two assumptions are considered: that only He + ions strike the divertor (magenta) and that only He2+ (green) ions strike the divertor. The cumulated time of the strike point position (#55813 to #55987) is also shown in dashed lines. (For interpretation of the references to colour in this figure legend, the reader is referred to the web version of this article.)

helium content is found in the inner and outer strike point areas following the helium campaign, with peaks at about 6 at.% in the ISP (s = 250 mm) and about 10 at.% in the OSP with a maximal He content at s = 395 mm. A third peak at s = 100–150 mm indicates the presence of helium (2 at.%) in the thick deposit area toward the HFS, where complex stratified layers made of W, C, O, B are found [12,27]. Almost no helium was found on the very HFS/LFS sides of the tiles.

In parallel with the He implantation depth profile, the cumulated particle fluence on the W/graphite PFUs inferred from the Langmuir probes and the position of the strike points reconstructed from the magnetic flux are shown in Fig. 3(b). Due to the diffusion into the scrape off layer, the values of 'Te' and 'n_e' could be slightly shifted from the position of the SPs. It is therefore not surprising to see that the position of the maximum fluence is slightly inboard of the ISP and outboard of the OSP. However, this shift is generally estimated to be a few millimeters. This effect appears consistent for the OSP in Fig. 3(b) but seems surprisingly large for the ISP.

The presence of helium in the OSP detected by IBA correlates well with the position of the SP and the fluence peak in this region. Depending on the hypothesis about the ratio of He ions striking the lower divertor (He^+ only or He^{2+} only), the cumulated fluence reaches between (2.5 and 5)x10^{24} He/m^2 at the OSP. This is sufficient to enable implantation and slightly exceeds the threshold of 10^{24} He/m^2 required for fuzz formation.

The results in the ISP are more intriguing. The helium peak at 6 at.% is not aligned with the position of the fluence peak but is more closely aligned with that of the SP, albeit by a few millimetres. This result remains unexplained.

In contrast, the He peak at 2 at.% can be easily explained by the very porous structure of the deposited layers, which facilitates helium retention even at very low fluences.

As for the ITER-like PFU, three He peaks can also be recognised in the implantation profile (Fig. 3(c)). One peak at the OSP, the most pronounced one at 5–6 at.%, one at the ISP with lower intensity, and a third, smaller peak, found in the deposited layers. Regarding the toroidal distribution of helium, monoblocks located at the ISP show relatively uniform helium amount over their surface, with values close to each other along the x-coordinate. However, monoblocks located at the OSP show a much more heterogeneous helium distribution (see section 3.4). MB 26, for example, shows a He content of 8x10^{20} at/m^2 at x = 4 mm and 2x10^{20} at/m^2 at x = -10 mm. Overall, the highest helium content is usually measured near the leading edge (x = 4 or 10 mm) at the OSP.

Because the ITER-like PFU was not equipped with LP, the He flux could not be measured directly. Instead, it was estimated from the W/graphite PFUs and by taking into account the particle flux modulation over the ripple. At the same time, it is difficult to estimate the time during which the W surface temperature exceeded 700°C. The same value as for the W/graphite PFUs (100 s) was therefore used, although it is clearly overestimated due to the fact that ITER-like PFUs are actively-cooled, making it more difficult to reach high temperatures at steady state. The calculated fluence is shown in Fig. 3(d). It can be seen, it is 2 to 3 times lower than for the W/graphite PFUs. At the OSP, the fluence is comprised between 0.8 to 1.5x10^{24} He/m^2 depending on the hypothesis about the ratio of He ions striking the lower divertor. Knowing that this value is overestimated, the fluence threshold of 10^{24} He/m^2 for fuzz formation becomes critical in that case.

Impact on W microstructure

W/graphite PFUs

In order to verify how the helium content evidenced in the W/graphite PFUs translates into microstructural changes in the W, the sample with the maximum helium content (s = 395 mm) was analyzed by electron microscopy. Low-magnification analysis of the sample

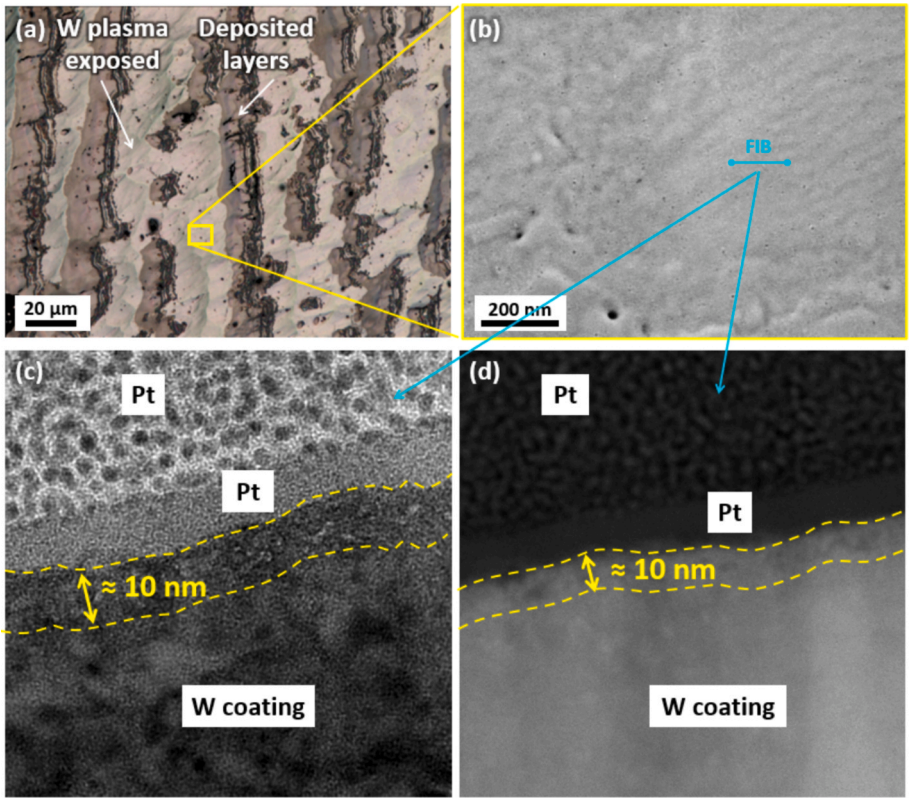

Fig. 4. (a) Optical image showing the surface of the W/graphite PFU sample with maximum helium content (s = 395 mm). (b) SEM image of the plasma-exposed area of the sample showing nanoporosities on the surface. Cross-sectional (c) TEM and (d) STEM images showing the presence of nanobubbles 10 nm underneath the surface of W coating.

(Fig. 4(a)) reveals two types of features on the surface: areas of erosion, where W is directly exposed to the plasma (i.e. to the helium flux), and areas of local redeposition (thickness of redeposited layers: 1–3 μm). As IBA measurement is performed on a millimeter-sized area, it averages the results over these 2 regions.

When examined at higher magnification, the tungsten area that has been exposed to plasma reveals the presence of nanopores (Fig. 4(b)), which are characteristic of helium exposure [28,29]. Cross-sectional images confirm that this nanoporosity is associated with bursting bubbles measuring 2–5 nm in diameter, located within the first 10 nm below the surface (Fig. 4(c,d)). The crystalline orientation in the STEM images indicates that these nanobubbles have formed in the W matrix and are not the result of a thin porous redeposited layer. Fuzz has not formed, but these nanobubbles are the precursors of it.

Bulk W ITER-like PFU

Figs. 5(a) and (b)Show the top surface of mb28 and its helium content along the toroidal direction, respectively. as stated before, the helium retention is quite heterogenous over the surface, with a peak at 9.2×10^{20} at/m^2 close to the leading edge (x = 10 mm), before gradually decreasing towards the trailing edge at x = -10 mm. Microstructural observations carried out in the region with highest helium content (x = 10 mm) (Fig.5 (c)) show the presence of nanobubbles in the W microstructure, 10 nm beneath the plasma-exposed surface, similar to the W/graphite PFUs. Additional observations were performed on the leading edge of MB26 (Fig. 5(d)) where a high content of helium was also measured ($8\text{x}10^{20}$ at/m^2 at x = 4 mm). Nanobubbles were also observed.

The presence of nanobubbles in ITER-like PFUs may seem surprising at first given that the temperature of the W monoblocks did not exceed 300-400°C [30], which is very low for helium uptake, in addition to the fact that the fluence was critically low. However, the ITER-like PFU was vertically misaligned, and the leading edge was directly exposed to the plasma, therefore to heat and particle fluxes. Temperatures > 900°C were locally reached on the leading edges [30] which could have promoted helium uptake and increased the chances of helium bubbles formation.

Discussion on helium depth implantation

The results of this study, obtained by TEM or TOF ERDA, highlight the presence of helium in the W, while revealing divergent implantation depths. For both W/graphite PFUs and ITER-like PFU, nanobubbles were found up to 10 nm beneath the surface by cross-sectional TEM.

According to SRIM [18], the maximum range of 150 eV, or even 300 eV, He ions in W at an incidence angle of 1.5° (ITER-like PFU) or 3.5° (W/graphite PFUs) is around 2 or 3 nm. The maximum He implantation depth is therefore 3 nm.

Of course, each of these techniques has its own specific features. TEM, for instance, is a highly localised technique that reveals only the 'visible'. Helium may have diffused deeper into the W without forming bubbles and that will not be visible by TEM. SRIM [18] is a Monte Carlo program based on the binary collision approximation used to calculate depth of the implanted ions. The program does not take into account possible diffusion of implanted He ions due to the implantation at high temperatures. Consequently, it does not necessarily represent rapidly evolving W in tokamak environment. TOF ERDA, on the other side, is a measurement averaged over several mm^2 of the sample surface, and therefore takes into account not only W plasma eroded parts but also redeposited layers of 1–3 μm visible on Fig. 4(a). Conversion from at/m^2 to nm is also challenging due to the unknown density of the material analysed. Nevertheless, there is a discrepancy with regard to the depth of the implantation (a few nm vs a few hundreds nm).

The results obtained by TOF ERDA indicate that He might be found below the implantation depth profile expected from SRIM, as shown in Fig. 2(b). However, as Fig. 4 (a) shows, the surface of the W/graphite PFU sample with maximum helium content (s = 395 mm) consists of two relatively well distinguished regions, W plasma exposed and deposited layers with a lateral roughness in the tenth of the micrometre range. Therefore we believe that Fig. 2(a) shows TOF ERDA spectrum which is sum of spectra from two distinct regions. However, the interpretation of TOF ERDA depth profile shown on Fig. 2 (b) is not straightforward as it would be if the spectrum is collected from only one region which is homogeneous. It was already demonstrated by M. Mayer [31] for case of RBS spectra that depth profiles from the laterally inhomogeneous materials can yield incorrect depth profiles, if interpreted as homogeneous material but total amounts of elements can be derived with some robustness from count integrals which is done in our case to calculate total amount of He. Therefore, total amounts of helium, as shown in Fig. 3, are more reliable than depth profiles.

Faney et al. [32] propose a model that could explain the detection of He deeper into W. They applied a cluster dynamic model to the case of high-flux helium irradiation typically encountered in fusion reactors. The novelty of the model lies in its ability to describe the evolution of tungsten microstructure due to very high incoming fluxes of helium ions (up to 10^{23} m^{-2} s^{-1}), resulting in rapid growth of large helium bubbles beneath the material's surface. For implantation of helium ions (E ≤ 100 eV) into a perfect tungsten surface with an infinite half-slab geometry, the model identifies different regimes depending on temperature. According to the model, for an implantation flux of $\varphi = 10^{22}$ m^{-2} s^{-1}, He ion energy ≤ 100 eV, temperature of 1000 K, and fluence up to 5×10^{23}

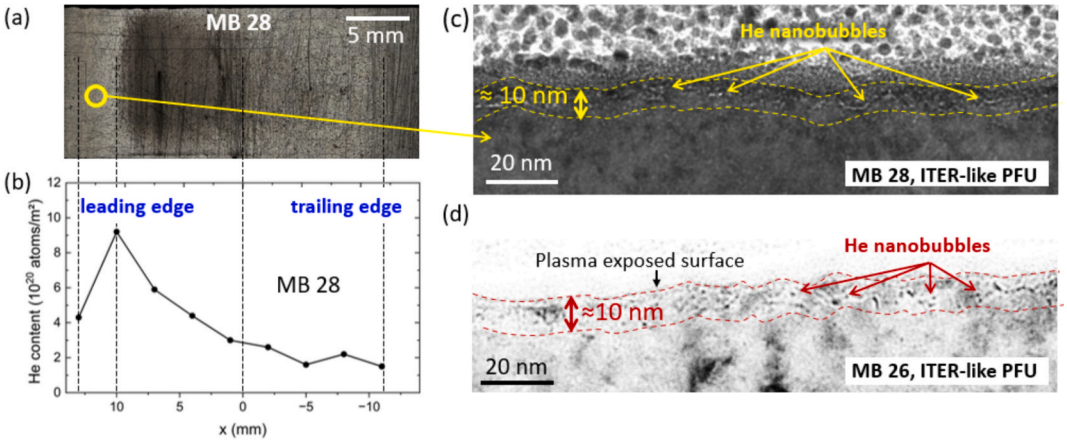

Fig. 5. (a) photograph of the top surface of MB28 and associated (b) helium content profile along the toroidal axis (x = 14 mm corresponding to the leading edge, x = -14 mm to the trailing edge). TEM cross-sectional images of (c) MB 28 and (d) MB 26, taken close to the leading edge (x = 12 mm) showing the presence of nanobubbles 10 nm underneath the surface of bulk W.

m^{-2}, the very high mobility of helium-interstitial atoms allows them to travel deep into the tungsten (several micrometres) within relatively short times. Beyond the implantation layer of a few nanometres, the concentration of helium-interstitial atoms is almost constant due to very fast helium diffusion in tungsten.

Self-trapping of helium atoms in the interstitial space creates mobile helium clusters that grow with increasing flux. As more He atoms are trapped and the clusters become larger, the immobile helium clusters and voids undergo a trap mutation process. The maximum concentration of these helium bubbles is initially located at ~200 nm below the surface. The helium bubbles act as a 'plug', preventing helium from diffusing deeper into the tungsten. The plug of large helium bubbles slowly moves towards the surface as incoming interstitial helium react at the front of the plug, while a decrease in the helium content is observed at the back of the plug. At the end, the plug is located approximately 50 nm below the surface, although it was initially formed several hundred nanometers below. Although we do not observe the end of the region with He bubbles at 50 nm, but rather at 10 nm, the model proposes a possible mechanism explaining the detection of He in deeper layers by TOF ERDA.

Conclusion

In this paper, interactions between W PFCs and helium plasma have been investigated through post-mortem analyses of divertor targets tiles recovered after a dedicated He campaign performed in the WEST tokamak in 2019 (C4 campaign). Both W-coated graphite PFUs and bulk W ITER-like PFU were investigated although the plasma scenario developed for this specific campaign was aimed to achieve the conditions necessary for fuzz formation ($T_{surf} > 700°C$, He fluence $> 10^{24}$ He/m^2 and incident He energy $>$ 20 eV) in the OSP area of W-coated graphite PFUs only.

The main conclusions of this paper are as follows:

- Helium was found to be mainly implanted in the ISP/OSP areas of the divertor targets, both in W coated graphite PFUs and bulk W ITER-like PFU. Some helium was also found in the thick deposited layers near the HFS, but in smaller quantities.
- The maximum helium content was found in the OSP area of the W/graphite PFUs (up to 10 at.%, s = 395 mm), proving the correct development of plasma scenarios (i.e correct position of the SP). In this area, a cumulated fluence of (2.5–5)x10^{24} He/m^2 was calculated over the estimated 100 s the W has reached 700°C. Despite favorable conditions, fuzz did not form but helium nanobubbles – the precursors of fuzz – are clearly visible underneath the surface. There are several possible reasons why fuzz did not form: i) the fluence is slightly too low, ii) 100 sec above 700°C is not long enough to form fuzz, iii) the start-up of fuzz is destroyed by erosion.
- In the OSP area of the investigated ITER-like PFU, the temperature of W did not exceed 300-400°C and the estimated fluence is very low, representing conditions not favourable to fuzz formation. Only the leading edge of the OSP monoblocks reached high temperatures (> 1000°C) with fluence probably high (but impossible to measure) due to the vertical misalignment of the component. It is in this region that helium bubbles were found underneath the surface.
- On all analyzed samples, helium implantation led to the formation of nanobubbles about 10 nm underneath the surface. Although bubbles are detected only in first 10 nm, He is found also in deeper layers according to TOF ERDA measurements.

CRediT authorship contribution statement

M. Diez: Writing – review & editing, Writing – original draft, Resources, Methodology, Investigation, Conceptualization. **C. Martin:** Writing – review & editing, Writing – original draft, Methodology, Investigation, Formal analysis. **A. Hakola:** Writing – review & editing, Methodology, Conceptualization. **A. Huart:** Writing – review & editing, Investigation, Conceptualization. **Y. Corre:** Writing – review & editing, Validation, Methodology, Conceptualization. **J. Gaspar:** Writing – review & editing, Investigation, Formal analysis. **Z. Siketić:** Writing – review & editing, Methodology, Formal analysis. **G. Giacometti:** Writing – review & editing, Methodology, Formal analysis. **T. Neisius:** Writing – review & editing, Methodology, Investigation, Formal analysis. **M. Cabié:** Writing – review & editing, Methodology, Investigation, Formal analysis. **Q. Tichit:** Writing – review & editing, Resources, Investigation, Conceptualization. **T. Vuoriheimo:** Writing – review & editing, Resources, Methodology. **A. Benmoumen:** Writing – review & editing, Methodology, Investigation, Formal analysis. **E. Tsitrone:** Writing – review & editing, Supervision, Resources, Methodology, Conceptualization. **I.Bogdanovic Radovic:** Writing – review & editing, Validation, Investigation.

Declaration of competing interest

The authors declare that they have no known competing financial interests or personal relationships that could have appeared to influence the work reported in this paper.

Acknowledgement

This work has been carried out within the framework of the EUROfusion Consortium, funded by the European Union via the Euratom Research and Training Programme (Grant Agreement No 101052200 — EUROfusion). Views and opinions expressed are however those of the author(s) only and do not necessarily reflect those of the European Union or the European Commission. Neither the European Union nor the European Commission can be held responsible for them.

Data availability

Data will be made available on request.

References

[1] A. Loarte, et al., Plasma Phys. Control. Fusion 67 (2025) 065023.
[2] S. Kajita, et al., J. Nucl. Mater. 548 (2021) 152844.
[3] M. Miyamoto, et al., J. Nucl. Mater. 415 (2011).
[4] K. Wang, et al., Sci. Rep. 7 (2017) 42315.
[5] G.M. Wright, et al., Nucl. Fusion 52 (2012) 042003.
[6] M. Rasinski, et al., Nucl. Mater. Energy 37 (2023) 101539.
[7] E. Tsitrone, et al., Nucl. Fusion 62 (2022) 076028.
[8] G. De Temmerman, et al., Nucl. Mater. Energy 19 (2019) 255–261.
[9] G. De Temmerman, et al., Plasma Phys. Control. Fusion 60 (2018) 044018.
[10] S. Kajita, et al., Nucl. Fusion 49 (2009) 095005.
[11] Y. Corre, et al., Fus. Engineering and Design 170 (2021) 112528.
[12] M. Diez, et al., Nucl. Mater. Energy 34 (2023) 101399.
[13] A. Grosjean, et al., Fus. Engineering and Design 168 (2021) 112387.
[14] A. Grosjean, et al., Nucl. Fusion 60 (2020) 106020.
[15] P. Tsavalas, et al., Nucl. Fusion 66 (2026) 036046.
[16] A. Marin, et al., J. Nucl. Mater. 604 (2025) 155525.
[17] M. Balden, et al., Nucl. Mater. Energy 46 (2026) 102081.
[18] W. Eckstein IPP-Report IPP-9/132 "Calculated Sputtering, reflection and range values", 2002.
[19] M. Sakamoto, et al., J. Nucl. Mater. 573 (2023) 154140.
[20] A. Wagner, et al., J. Nucl. Mater. 473 (2016) 163–170.
[21] E. Grigore, et al., Surf. Coat. Technol. 376 (2019) 21–24.
[22] I. Jogi, et al., Nucl. Mater. Energy 39 (2024) 101677.
[23] H.J. van der Meiden, et al., Nucl. Fusion 61 (2021) 125001.
[24] Z. Siketić, et al., Nucl. Inst. Methods Phys. Res. B 266 (2008) 1328–1332.
[25] Z. Siketić, et al., Rev. Sci. Instrum. 86 (2015) 083301-1.
[26] K. Arstila, et al., Nucl. Instr. and Meth. B 331 (2014) 34–41.
[27] M. Balden, et al., Phys. Scr. 96 (2021) 124020.
[28] M. Alfazzaa, et al., Nucl. Mater. Energy 42 (2025) 101883.
[29] M. Ialovega, et al., Nucl. Fusion 62 (2022) 126022.
[30] M. Diez, et al., Nucl. Mater. Energy 41 (2024) 101746.
[31] M. Mayer, et al., Nucl. Instr. and Meth. B 371 (2016) 90–96.
[32] T. Faney, S.I. Krasheninnikov, B.D. Wirth, Nucl. Fusion 55 (2015) 013014.